International Journal of Bifurcation and Chaos, Vol. 29, No. 8 (2019) 1930021 (14 pages)
© World Scientific Publishing Company
DOI: 10.1142/S0218127419300210

Gap Junction Dynamics Induces Localized Conductance Bistability in Cardiac Tissue

C. Hawks*, J. Elorza*, A. Witt†, D. Laroze‡, I. R. Cantalapiedra§, A. Peñaranda§, B. Echebarria§ and J. Bragard*,¶

*Department of Physics and Applied Mathematics, University of Navarra, E-31080 Pamplona, Spain

†Biomedical Physics Group, Max Planck Institute for Dynamics and Self-Organization, Göttingen, Germany

‡Instituto de Alta Investigación, CEDENNA, Universidad de Tarapacá, Casilla 7D, Arica, Chile

§Departament de Física, Universitat Politècnica de Catalunya, EPSEB, Barcelona, Spain

¶jbragard@unav.es

Received November 2, 2018; Revised January 16, 2019

Connexins are specialized ionic channels that control the action potential propagation between cardiac myocytes. In this paper, we study the connexin dynamics in a one-dimensional model of cardiac tissue. We show that the connexin dynamics may lead to a spatial organization of the gap junction conductance. In the numerical simulations presented in this paper we have found two different regimes for the spatial organization of the conductances: (a) a spatially uniform conductance; (b) a spatially complex pattern of local values of high and low conductances. In addition, we have observed that, locally, the two final states are limit cycles with a period equal to the period associated with the external excitation of the tissue strand. The conductance dispersion usually takes place on a very large time scale, i.e. thousands of heart beats, and on a very short spatial scale. Due to its simplicity, the one-dimensional setting allows a detailed study of the emerging structure and in particular very long simulations. We have studied the transition between the two aforementioned states as a function of the gap junction conductance characteristics. Furthermore, we have studied the effect of initially added noises on the outcome of the system. Finally, using spatial autocorrelation functions we have characterized the spatial dispersion in conductance values.

Keywords: Cardiac dynamics; gap junction dynamics; connexins Cx43-43; bistability; chaotic dispersion.

1. Introduction

The description of the electrical activity in the cardiac tissue is still a field of research in applied mathematics and bioengineering [Cherry *et al.*, 2017; Gokhale *et al.*, 2017]. Most models describe the electrical wave that travels across the cardiac tissue and triggers the mechanical contraction of the heart. The first generation of mathematical models for the description of the cardiac wave propagation uses constant values for the conductances between adjacent myocytes as a simplified hypothesis. This approximation resulted in a constant diffusive term in the partial differential equation that describes the dynamics of the transmembrane potential,

i.e., classical nonlinear reaction–diffusion equation. This equation is called the "monodomain" equation in the cardiac modeling literature [Keener & Sneyd, 1998; Sachse, 2004].

Nowadays, more complex situations like defibrillation studies or local damage of the cardiac tissue [Schulz *et al.*, 2015] require a more accurate description of the spatial distribution of the conductance between myocytes. In cardiac tissue, adjacent cells are joined through gap junctions (Fig. 1), that allow the transport of ions among cells, resulting in diffusion of the transmembrane potential. A detailed description of electrical wave propagation needs to take into account the gap junction dynamics, that has been well characterized experimentally [Vogel & Weingart, 1998; Desplantez *et al.*, 2004, 2007; Willy *et al.*, 2017; Santos-Miranda *et al.*, 2018]. Structurally, gap junctions are composed of connexin proteins. In mammals, the most common type of connexins in cardiac cells are the Cx43 and Cx45 (the number in the denomination of the protein comes associated with its molecular weight).

There is increasing evidence that alterations of gap junction organization and connexin expression are related to human heart disease and arrhythmias [Jalife *et al.*, 1999; Delmar & Makita, 2012; Tse & Yeo, 2015; Boengler & Schulz, 2018]. In this sense, a reduction of expression of Cx43 in ventricles has been observed in patients with ischemic cardiomyopathy and other chronic myocardial disease states [Severs *et al.*, 2008]. In failing hearts, one of the consequences of the observed down-regulation of Cx43 expression is conduction slowing [Kostin *et al.*, 2003; Glukhov *et al.*, 2012]. Hypertrophic and dilated cardiomyopathy produces also a rearrangement of connexin Cx43, leading to a heterogeneous connexin redistribution and down-regulation expression resulting in conduction defects [Gutstein *et al.*, 2001]. Mutations that produce changes in connexin phosphorylation affect also the functionality of channels and the conductance of gap junctions [Imanaga, 2010]. Phosphorylation of Cx43 may increase the size of gap junctions, promoting cell to cell communication [Dunn & Lampe, 2014]. An experimental study by Beardslee *et al.* [2000] has put forward the connection between ischemic hearts and the remodeling of the cardiac electrical conductance through the dephosphorylation of ventricular Cx43. Furthermore, mutations of connexin proteins have been implicated in the pathogenesis of sudden infant death syndrome [Van Norstrand *et al.*, 2012] and in atrial fibrillation [Noureldin *et al.*, 2018]. Consequently, pathological remodeling of connexins contributes to arrhythmogenic substrates and development of reentrant arrhythmias.

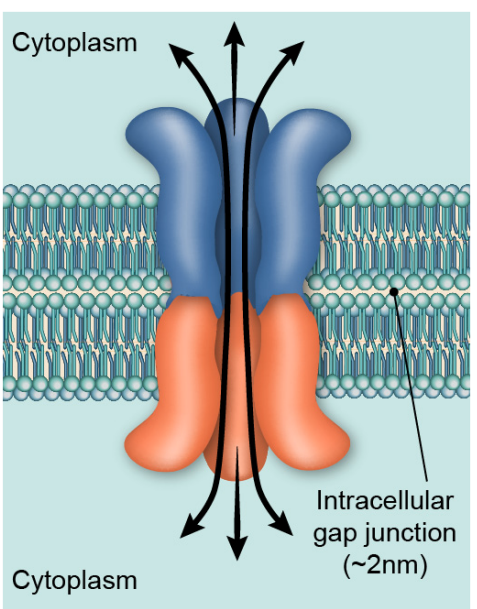

Fig. 1. Illustration of the structure and functionality of a gap junction (GJ) connecting electrically two cardiac myocytes. The thickness of the bilipidic layer is of the order of a few nanometers. The ions can flow in both directions through the GJ. This figure has been taken from [Beutler, 2018].

Due to its physiological relevance, the effect of intercellular coupling has long been addressed computationally. A modeling study combining reduced membrane excitability and reduced gap junction coupling by Shaw and Rudy [1997] concluded that paradoxically a decreased gap junction coupling may increase the propagation safety factor. The inclusion of the gap junction dynamics has been studied in a modeling paper by Hand and Griffith [2010] that applies a multiscale approach combining microstructure details and macroscopic tissue characteristics. In the same line of ideas, Costa *et al.* [2016] developed a semi-continuous model for the description of the electrical propagation in the cardiac tissue, including the gap junction dynamics. A different modeling perspective consists in considering the heart as a network of different types of cells which are electrotonically coupled via gap junctional conductance [Qu, 2014]. In normal ventricular tissue, a myocyte is coupled to about 11 myocytes, which is reduced to about six in ischemic tissue [Peters & Wit, 1998]. The study of the topology of

those networks for healthy and diseased individuals is still an active field of research. Recently, Cantalapiedra *et al.* [2014] developed a model combining a membrane description of the cardiac myocytes supplemented with a local gap junction dynamics to study gap junction dysregulations.

The purpose of this paper is to show that the inclusion of the gap junction dynamics can lead to strong variations in the values of the conductances. We will show that, on long time scales, it can lead to a drastic decrease in conductance values and, interestingly, to nontrivial spatial distributions of the electrical conductances in the cardiac tissue. In these situations, the approximation of a constant, homogeneous conductance, usually considered in modeling studies of cardiac wave propagation, leads to invalid results. The organization of the paper is as follows: In Sec. 2, we provide the model description. The simulations of the model are presented and analyzed in Sec. 3. In particular, we study in detail the spatial distribution found for the conductances. Finally, discussions of the limitations and the conclusions are given in Sec. 4.

2. Model Equations

A previous study [Hawks *et al.*, 2015] already showed that the difference between a monodomain and a bidomain formulation [Keener & Sneyd, 1998] was negligible to study the long term effect of the variation of the tissue conductance induced by the GJ dynamics. Based on that, we will use a monodomain formulation of electrical wave propagation, and present here the ingredients of the model used in the current study.

2.1. *Monodomain formalism*

Let us first remember the monodomain equations [Keener & Sneyd, 1998; Sachse, 2004]:

$$\frac{\partial s}{\partial t} = f(V, s), \tag{1}$$

$$\frac{\partial V}{\partial t} + \frac{I_m + I_{\text{ext}}}{\mathcal{C}} = \nabla \cdot (D \nabla V), \tag{2}$$

where s is the dynamical state vector that contains all the variables involved in the local description of the ionic currents crossing the myocyte membrane. The vector function $f(V, s)$ in Eq. (1) is a highly nonlinear phenomenological function that is measured through biophysical cell experiments [Keener & Sneyd, 1998]. V denotes the transmembrane potential (units are in mV), I_m is the sum of the ionic currents (units are $\mu\text{A/cm}^2$) and $\mathcal{C}$ is the membrane capacitance per unit area ($\approx 1\,\mu\text{F/cm}^2$). The term I_{ext} allows for the introduction of an external current as it happens during an external excitation of the cardiac tissue. The tissue diffusion $D = \sigma/(\beta\mathcal{C})$ is the ratio between the electrical conductivity σ (units are mS/cm) and the product $(\mathcal{C}\,\beta)$ where the latter denotes the average surface to volume ratio of the myocyte (units are cm^{-1}). Typical values in mammalian cells lead to a diffusion value of approximately $D \approx 1.5 \cdot 10^{-3}\,\text{cm}^2/\text{ms}$ [Aguel *et al.*, 2003]. Note that the time scales associated with Eqs. (1) and (2) vary from 0.1 ms up to 1 s and even higher. Consequently, the differential equations (1)–(2) are stiff and their numerical integrations are challenging.

2.2. *Gap junction dynamics*

When one includes the GJ dynamics, the assumption of constant homogeneous conductivity no longer holds and instead we have to write that $D = D(\mathbf{x}, t)$. The coupling between the GJ dynamics and the action potential propagation may lead to some interesting dynamical bistability [Donnell *et al.*, 2009]. Here, the dynamics of the gap junctions is modeled as proposed in the papers of Lin *et al.* [2003] and Desplantez *et al.* [2004]. The relation between the conductance and the GJ dynamical function g is simply written as follows:

$$D(\mathbf{x}, t) = \overline{D} g_{\mathbf{x}}(t), \tag{3}$$

where $\overline{D}$ is the fixed nominal value for the intracellular conductivity and $\overline{D} = 1.5 \cdot 10^{-3}\,\text{cm}^2/\text{ms}$ for a healthy tissue.

To simplify the problem we will work in a one-dimensional spatial system. Therefore, when we discretize space in order to solve the model [Eqs. (1) and (2)], the index number i corresponds to the cell number i on the cable. The index number i also corresponds to the gap junction g_i situated between cell number $i-1$ and cell number i. At each location, we need to solve the gap junction dynamics, which is governed by the following set of differential equations:

$$\frac{dg_i}{dt} = \frac{g_{i,ss}(\Delta\phi) - g_i}{\tau_g(\Delta\phi)}, \tag{4}$$

where $\Delta\phi = \phi(i) - \phi(i-1)$ is the difference in intracellular electrical potential between the two adjacent cells of g_i. The steady state value in Eq. (4)

Table 1. Values for the Gap Junction dynamics. Here, the parameter values are indicated for ($\Delta\phi < 0/\Delta\phi \geq 0$).

Connexin Type	$V_{1/2}$ (mV)	$g_{i,\min}$	z
Cx43_43	−60.8/62.9	0.26/0.25	−3.4/2.9
Cx43_45	−11.7/134.4	0.05/0.05	−2.1/0.6
Cx45_43	134.4/−11.7	0.05/0.05	0.6/−2.1

depends on the local instantaneous $\Delta\phi$ following this equation:

$$g_{i,ss} = \frac{g_{i,\max} - g_{i,\min}}{1 + \exp[A(\Delta\phi - V_{1/2})]} + g_{i,\min} \qquad (5)$$

and the time scale in Eq. (4) is given by $\tau_g = A_\tau \exp[-B_\tau|\Delta\phi|]$. The parameter values entering Eqs. (4) and (5) are taken from the works of Lin *et al.* [2003] and Desplantez *et al.* [2004]. They are given in Table 1.

We also have the following relations for the parameter values: $A = z/26.714$ $(\text{mV})^{-1}$; $A_\tau = 109\,900$ (ms); $B_\tau = 1/11.8$ $(\text{mV})^{-1}$; $g_{i,\max}(\Delta\phi = 0) = 1$. The dependence of $g_{i,ss}$ as a function of $\Delta\phi$ is displayed in Fig. 2. In this study, we will use only the symmetric GJ of type (Cx43_43) described above.

We emphasize that because we are using a monodomain formulation, the computation of the term $\Delta\phi = \phi(i) - \phi(i-1)$ reduces to $\Delta V = V(i) - V(i-1)$ as a result of assuming that the extracellular electrical potential is constant throughout the domain.

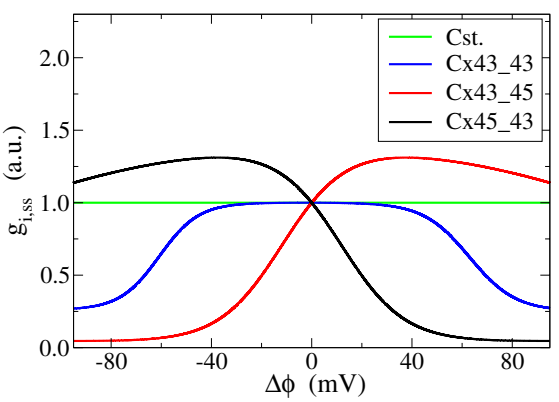

Fig. 2. Steady state values of the gap junction $g_{i,ss}$ [see Eq. (4)] as a function of the difference in intra-cellular electrical potential between adjacent cells, $\Delta\phi$, for the different types of gap junctions. The labels indicate the connexin types that conform with different GJ. The horizontal line (green) represents the case where the conductance is assumed constant.

2.3. *Transmembrane model selection*

In order to describe the electrical propagation of the action potentials through our system we need to select an adequate description of the transmembrane currents. Since the 1960s, many differential-equations-based models that describe the kinetics of the cell membrane have been developed [Keener & Sneyd, 1998; Sachse, 2004]. In some cases, models have evolved to become quite complex by representing cellular processes in detail [Grandi *et al.*, 2010]. Other models, e.g. the three-variable Fenton and Karma model [1998], represent quite faithfully the propagation of the action potential without the numerical burden associated with the large numbers of variables in the more complex models. In 2010, Cantalapiedra *et al.* [2010, 2014] developed a generic five-variable model containing a specific formulation for the transient outward K^+ current, which is important in describing action potentials associated with the Brugada syndrome. In this paper, we use the Cantalapiedra *et al.* model [2010, 2014] with the model parameter fitted to describe human ventricular myocytes [Ten Tusscher *et al.*, 2004].

2.4. *Numerical methods*

A one-dimensional strand of a ventricular cardiac tissue was simulated using Eqs. (1)–(4). Time and space were discretized using $\delta x = 0.01$ cm and $\delta t = 0.01$ ms. We use a simple Euler explicit scheme to integrate the set of Eqs. (1)–(4). In particular, Eq. (2) is discretized as follows:

$$V^{(n+1)}(i) = V^{(n)}(i) + \overline{D}\frac{\delta t}{\delta x^2}\{g_{i+1}^{(n)}[V^{(n)}(i+1) - V^{(n)}(i)] - g_i^{(n)}[V^{(n)}(i) - V^{(n)}(i-1)]\} - \delta t\frac{I_m^{(n)} + I_{\text{ext}}^{(n)}}{\mathcal{C}}, \qquad (6)$$

where the superscript (n) refers to variables taken at time step n. Here we consider that the size of the myocytes is constant and corresponds to one $\delta x = 100\,\mu$m. Therefore one GJ is always located in between two spatial grid points, i.e. g_i is the GJ situated between cell number $i-1$ and cell number i. This is the same as assuming that the cells are isopotential and all the drop in transmembrane

potential occurs at the gap junctions [Keener, 1991]. The discretization scheme of Eq. (6) follows from a finite volume method and as such ensures the current conservation up to machine precision. The extension of the one-dimensional strand of cardiac tissue that we have considered here was set to $N = 400$ cardiac myocytes. We have checked that the δt we have chosen is sufficiently small to ensure that the numerical results are robust and the numerical error is less than 0.5%.

The dynamics of the GJ is studied following the stimulation protocol as described below: We excite periodically the strand of tissue at one end by injecting current in order to elicit an action potential. In particular, the first seven cells of the strand are stimulated for 1 ms with an excitation current of $I_{\text{ext}} = 0.52\,\mu\text{A/cm}^2$. Following this excitation, an action potential (AP) is elicited. Note that a larger current would be needed to elicit an AP if fewer cells were excited. After initiation, the AP propagates towards the opposite end of the cardiac strand of tissue. We repeat the stimulation periodically in time. For all the simulations presented in this paper we have fixed the excitation period to $T = 480$ ms. Most of the simulations presented in this paper require a large number of excitations in order to display nontrivial dynamics. In some cases we have performed simulations that required as much as 10 000 excitations (or over 1 h) to reach a steady state for the GJ dynamics.

3. Results of the Model

In healthy tissue, the parameters associated with the membrane model and the connexins are such that the conductance is nearly uniform in space and constant in time as it has been shown previously [Cantalapiedra *et al.*, 2014].

In some diseased tissue, it has been observed that the average conductance can be dramatically reduced [Verheule & Kaese, 2013; Asimaki & Saffitz, 2012] and also that the time scale associated with the connexin is altered [Spach *et al.*, 2000], for instance due to drug intake [Hsieh *et al.*, 2016], an increase in fibrosis content [Sachse *et al.*, 2008], temperature [Santos-Miranda *et al.*, 2018] or connexin mutations [Noureldin *et al.*, 2018]. In this paper, we aim at simulating a diseased tissue and looking at the effect of the connexin dynamics on the conductance distribution. In particular, we show that complex one-dimensional conductance structures develop upon stimulating the tissue for altered

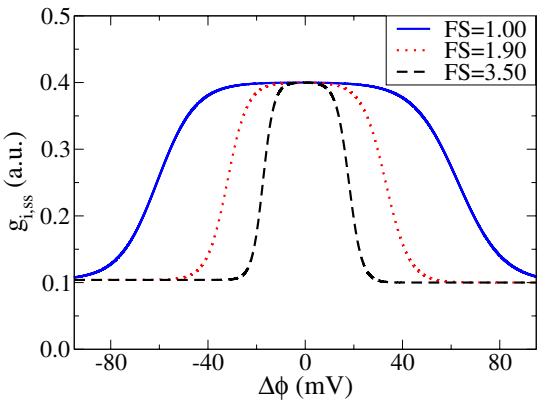

Fig. 3. Steady state values of the gap junction $g_{i,ss}$ of type (Cx43_43) as a function of $\Delta\phi$ for three different values of FS ("Shrinking factor"): FS = 1 (blue solid line); FS = 1.9 (red dotted line); FS = 3.5 (black dashed line). For modeling diseased tissue note that the maximum values for the $g_{i,ss}$ has been reduced to 40% of their nominal values.

parameters of the model. Here we have performed simulations with values of the conductance that are set to a maximum of 40% of their nominal values ($g_{i,\max}(\Delta\phi = 0) = 0.4$). We have also reduced the time scale by modifying the parameter to this new value $B_\tau = 1/5\ (\text{mV})^{-1}$. A last modification to the model was to introduce a parameter associated with the steady state characteristics of the GJ conductance ($g_{i,ss}$). We have called this parameter the shrinking factor FS which is directly related to the width of the plateau characterizing the GJ dynamics as shown in Fig. 3. Experimental evidences of varying GJ characteristics can be found in [Bennett *et al.*, 1991; Bukauskas *et al.*, 2002].

3.1. *Bistability induced by the shrinking factor FS*

In this section, we explore the influence of the shrinking factor FS on the final state of the conductance. In order to do this, we set different values for FS and observe the resulting dynamics in space-time plots (see Fig. 4). A more comprehensive study of the bifurcation induced by the parameter FS will follow (see Fig. 7). Figure 4 displays the spatiotemporal dynamics of the GJ for five selected values of the shrinking factor. In Fig. 4(a), which corresponds to the "normal value" for the shrinking factor, i.e. FS = 1, we observe that the dynamics leads to a spatially uniform value for the conductance g close to the maximum value which is set here to $g \approx 0.4$. In Figs. 4(b)–4(d), we have found out that intermediate values of FS ($1 < \text{FS} < 5$)

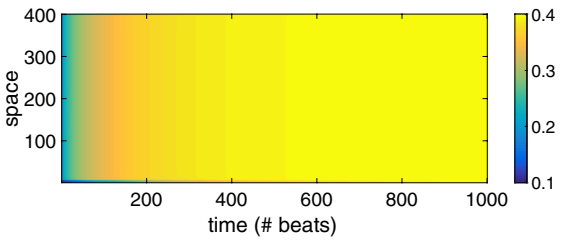

(a)

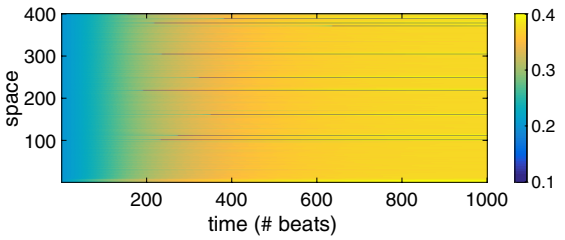

(b)

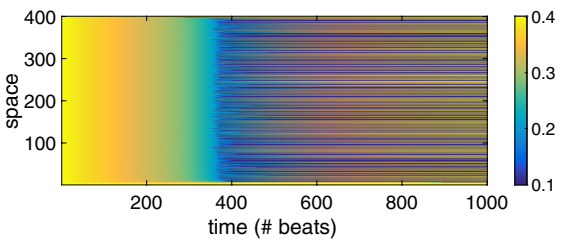

(c)

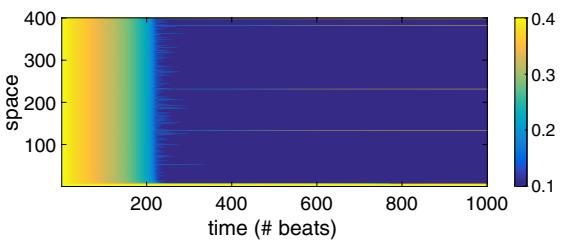

(d)

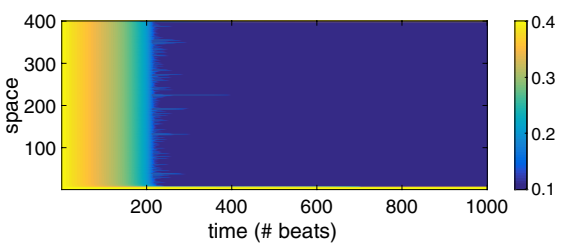

(e)

Fig. 4. Illustrative space-time plots of the conductance g of the symmetrical GJ Cx43_43 taken at regular time intervals ($T = 480$ ms). The color code represents the local values of the conductance (a.u.). The five different cases shown refer to the following shrinking factors FS: (a) FS = 1.0; (b) FS = 1.44; (c) FS = 1.9; (d) FS = 3.5 and (e) FS = 20.

lead to nontrivial final spatial distribution of the conductance values (g_i). We observe alternations of high and low values of the conductance. The density of low conductance states increases while increasing the value of FS. Furthermore, the pattern of alternations between high and low conductances is not regular but spatially disordered. Finally, for large values of the FS, after a transient, we get a spatially uniform conductance g which is now close to the lower value of the GJ characteristics, i.e. $g \approx 0.1$ as shown in Fig. 4(e) for the parameter value FS = 20.

These preliminary results indicate that we have found evidences for a transition induced by the increase (or decrease) of the parameter FS. This transition is between the upper uniform conductance $g \approx 0.4$ to the lower uniform conductance $g \approx 0.1$, resembling the dynamic conductance down regulation, recently observed in experiments [Willy *et al.*, 2017]. In between these two limiting cases we observed [see Fig. 4(c)] an irregular spatial pattern of high and low conductances where the two states are mixed.

Let us now analyze in more detail the mixed state that corresponds to intermediate strengths of the shrinking factor FS. From Fig. 5, we observe that the gap junction values bifurcate near the 400th beat and then converge to two different states with high and low average conductance values.

At a first glance Fig. 5 may be misleading because it seems that the two neighboring gap junctions are converging to two fixed points (conductance at approximately 40% and 10% of the homeostatic conditions). Instead, a closer look at the temporal dynamics as displayed in Fig. 6 shows that

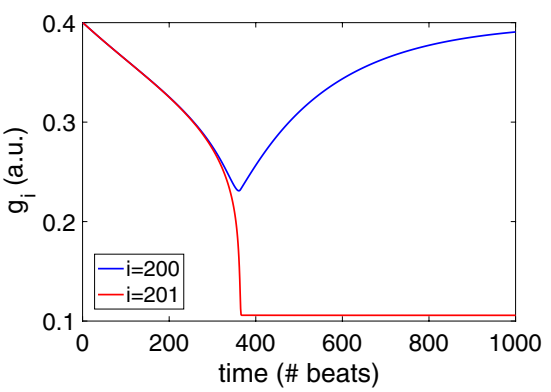

Fig. 5. Two horizontal cuts of Fig. 4(c) (with shrinking factor FS = 1.9) at two consecutive spatial positions corresponding to grid points $i = 200$ and $i = 201$. Note that near the 400th beat, the conductance of the two neighboring gap junctions starts to diverge.

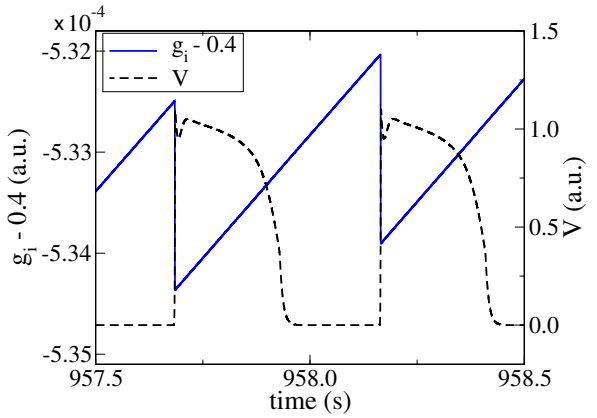

(a)

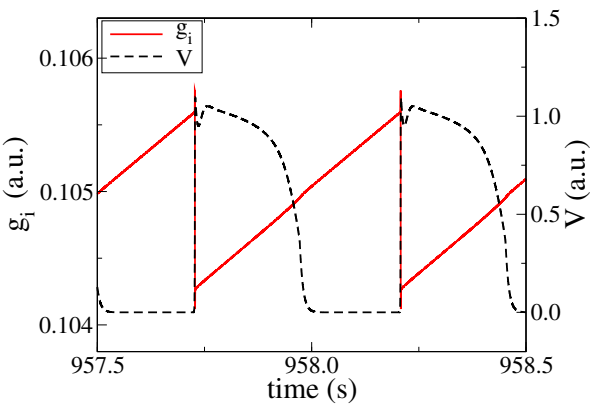

(b)

Fig. 6. Close up of the dynamics shown in Fig. 5 showing the time evolution of the gap junctions g_i and of the action potentials V_i at the two locations (a) $i = 200$ and (b) $i = 201$. Locally, the gap junction conductance is converging towards one of the two periodic states: (a) the upper state or (b) the lower state. Parameter FS is fixed as 1.9. Note that the left vertical axis in panel (a) is shifted downward by 0.4 in order to highlight the convergence to the upper state.

the two neighboring gap junctions are converging to two different periodic states. In Fig. 6(a), we focus on the upper value of the conductance close to the value $g_i \approx 0.4$. In order to represent the GJ variations accurately we shift the vertical axis $(g_i - 0.4)$ and also superimpose the plot of the membrane action potential (AP) with its normalized scale on the left vertical axis. In Fig. 6(b), we focus on the lower value of the conductance close to the value $g_i \approx 0.1$. Again we see that over a period, the conductance of the GJ drops significantly when the AP depolarizes and increases rather constantly for the rest of the period. The temporal dynamics unfolds on two time scales. One is associated with the stimulation period (BCL = 480 ms) and the other one with the membrane depolarization at a scale of the order of 1 ms.

For a first quantitative analysis of the GJ model, we have studied the influence of both, FS and the initial value for the conductances $g_{\rm ini}$, for characterizing the transition between upper and lower states of the conductance. We define an order parameter to characterize this transition by choosing the average value for the conductance $\langle g \rangle$ when it converges to its corresponding limit cycle. In Fig. 7, we show how $\langle g \rangle$ varies as a function of FS for three different values of the initial conductance in the system: $g_{\rm ini} = 0.1$ (blue triangle symbols); $g_{\rm ini} = 0.52$ (red circle symbols); $g_{\rm ini} = 0.4$ (green diamond symbols). We found an excellent agreement between the numerical data and their fitting curves with hyperbolic tangent functions. This is reminiscent of a second order phase transition. The explicit function for the fitting is given by

$$\langle g \rangle = \bar{g} + 0.5 \Delta g \tanh[w(\mathrm{FS}^* - \mathrm{FS})], \qquad (7)$$

where the best fit parameters and their corresponding confidence intervals are given in Table 2.

From Fig. 7, we see that the transition between the upper and lower values for the GJ conductance depends on the initial value set in the simulation. This will be studied in detail in Sec. 3.2.

Before investigating that, let us first explain why the transition takes place. As shown in Figs. 6(a) and 6(b) the connexin dynamics acts on two time scales. During the depolarization, $\Delta\phi$ is large and negative and therefore the g_i decreases

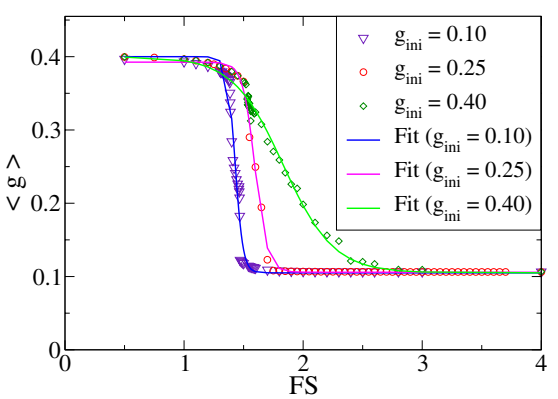

Fig. 7. Variation of the mean value of the conductance $\langle g \rangle$ as a function of the shrinking factor FS. There are three sets of data (and their best fitting hyperbolic tangent functions) corresponding to three different sets of initial values for the conductances: $g_{\rm ini} = 0.1$ (blue triangles); $g_{\rm ini} = 0.25$ (red circles); $g_{\rm ini} = 0.4$ (green diamonds).

Table 2. Values for the fitting parameters associated with Eq. (7). The 95% confidence bounds are also indicated in the table (in parentheses) as well as the adjusted R^2 characterizing the goodness of the fit.

$g_{\rm ini}$	$\bar{g}$	Δg	w	FS*	R^2
0.10	0.2496	0.2854	16.09	1.432	0.977
–	(0.2422, 0.2570)	(0.2693, 0.3016)	(13.43, 18.75)	(1.42, 1.44)	
0.25	0.2492	0.2867	9.711	1.595	0.998
–	(0.2473, 0.2512)	(0.2828, 0.2907)	(8.90, 10.52)	(1.59, 1.60)	
0.40	0.2597	0.3011	2.258	1.801	0.992
–	(0.2538, 0.2656)	(0.2861, 0.3162)	(2.03, 2.486)	(1.77, 1.83)	

according to Eq. (4), but this decrease lasts only a few milliseconds. For the remaining time of the excitation cycle $\Delta\phi$ is small and positive and g_i grows back to the maximum value (here $g_i \approx 0.4$). This tug-of-war between the depolarization phase trying to reduce g_i and the repolarization phase tending to increase g_i is mediated by the shrinking factor FS. Furthermore, since the time scale $\tau_g(\Delta\phi)$ is also dependent on $\Delta\phi$, that will confer an advantage for the depolarization by reducing the time scale in Eq. (4). To fully understand the transition, as shown by the example in Fig. 4(e) for FS = 20, we need to introduce two additional equations. First, we will assume that in the first order approximation we have the following relation between the local action propagation speed c_i and the local value of the conductance [Keener & Sneyd, 1998]:

$$c_i \propto \sqrt{g_i}. \tag{8}$$

Secondly, we will define the "residence time" $\tilde{\Delta}t$ which is the time for the action potential to move from one cell to the next cell in the cable. By using standard kinematic consideration we can write that:

$$\tilde{\Delta}t_i = \frac{\delta x}{c_i}, \tag{9}$$

where δx is the distance between two cells. In writing Eq. (9) we have assumed that the action potential propagates keeping a fixed morphology. At this point we have all the ingredients we need to explain why the system is transitioning to the lower state $g_i \approx 0.1$ when we set large values for FS. We have a positive feedback loop that induces a decrease in g_i during the depolarization phase that is never recovered during the rest of the period. In Fig. 8, we illustrate the three steps of this positive feedback loop: due to Eq. (4) the g_i decreases during the depolarization; due to Eq. (8) the local corresponding speed is also reduced; through Eq. (9) that induces an increase in the "residence time" $\tilde{\Delta}t$ and the loop is closed. The g_i will decrease until they reach their minimum values $g_i \approx 0.1$. Note that if FS is not as large, the recovering period is sufficient to bring back g_i to higher values close to $g_i \approx 0.4$, as shown in Fig. 4(a).

A second question that immediately comes to mind is why the intermediate values of FS give rise to a spatially disorganized pattern of nearly alternating up and down states. This can be explained by using the fact that the action potential propagates in a saltatory fashion. Indeed, a close look at the simulations show that if the local speed of the AP is reduced then at the next cell the speed is usually much larger. Invoking again Fig. 8 a large speed will lead to a local decrease in the "residence time" $\tilde{\Delta}t$ and the g_i will recover (through the repolarization phase) and locally tend to the upper state $g_i \approx 0.4$. These spatial alternans of up and down states in the conductance values are therefore a direct consequence of the nonlocality of the AP speed. In order to get a better insight of the crucial influence of the local "residence time" $\tilde{\Delta}t_i$ in the outcome of the final state of the g_i, the reader may have a look at the phase space animations at this Web page [Bragard, 2018].

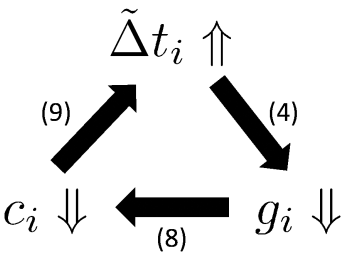

Fig. 8. Positive feedback loop during the depolarization phase. The up and down arrows mean an increase or a decrease of the indicated variable. The number next to each arrow refers to the equation in the text that justifies the logical step in the feedback loop.

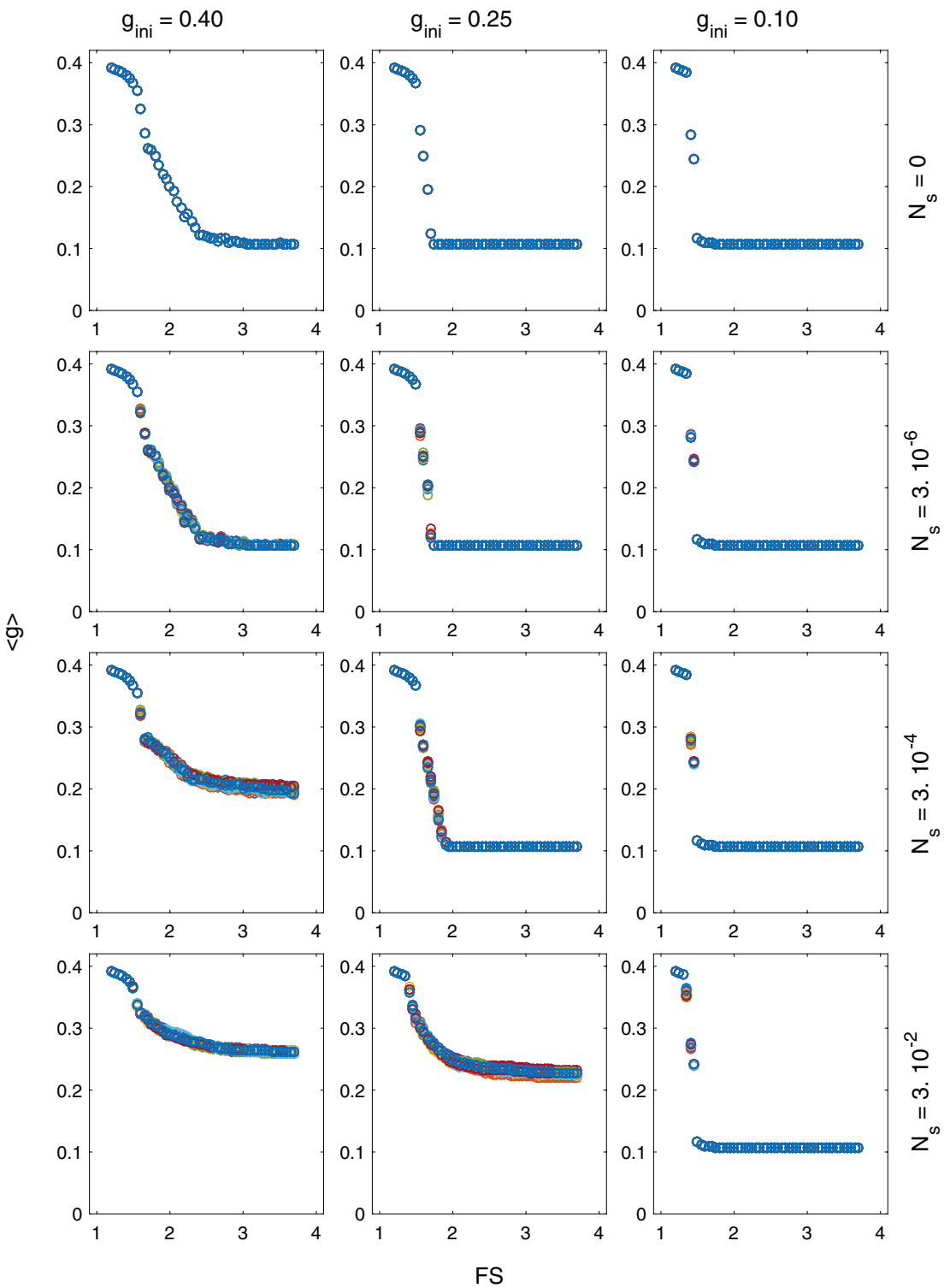

Fig. 9. Composite figure in each panel shows the spatial mean of the conductance values $\langle g \rangle$ (vertical axis) as a function of the shrinking factor FS (horizontal axis). Two parameters are associated with each panel. The noise strength is varied with the panel's row: $N_s = \{0; 3 \cdot 10^{-6}; 3 \cdot 10^{-4}; 3 \cdot 10^{-2}\}$ (top to bottom). The initial GJ value g_{ini} is varied with the panel's column: $g_{\text{ini}} = \{0.4; 0.25; 0.1\}$ (left to right). The different colored symbols represent different random realizations of the initial added noise. Here we have used 15 independent random realizations for each set of parameters.

3.2. *Influence of the initial conductance to the bistable regime*

In this section, we return to the numerical simulations of Eqs. (4) and we introduce a new parameter to the problem. We will study the influence of the noise that is added to the mean initial value of the conductance $g_{\rm ini}$. We have set $g_i^{(0)}$, with i the spatial index associated to the GJ, as follows:

$$g_i^{(0)} = g_{\rm ini} + N_s \sigma_u, \tag{10}$$

where σ_u is a uniform random variable distributed in the interval $[-1;1]$ and N_s is the parameter that characterizes the noise strength in the initial condition.

With the panels of Fig. 9 we can analyze at a glance the effect of varying simultaneously the three crucial parameters in the model, that is: FS, $g_{\rm ini}$ and N_s. Their variations are reflected in the variation of the order parameter characterizing the bifurcation, i.e. the mean of the GJ conductance $\langle g \rangle$. Note that to compute the spatial mean $\langle g \rangle$ we have always discarded the 20 cells closer to the boundaries in order to avoid spurious boundary influences. In Fig. 9, we have selected three values for the initial conductances, i.e. $g_{\rm ini} = \{0.4; 0.25; 0.1\}$ (columns, left to right). We have studied four values for the added noise strength, i.e. $N_s = \{0; 3 \cdot 10^{-6}; 3 \cdot 10^{-4}; 3 \cdot 10^{-2}\}$ (rows, top to bottom). In Fig. 9, we observe the dependence of $\langle g \rangle$ as a function of FS in each case. Figure 9 indicates that the transition is indeed dependent on both, the initial value $g_{\rm ini}$ and the noise strength N_s. For initial values of $(g_{\rm ini} = 0.4, N_s = 3 \cdot 10^{-2})$, $(g_{\rm ini} = 0.4, N_s = 3 \cdot 10^{-4})$ and $(g_{\rm ini} = 0.25, N_s = 3 \cdot 10^{-2})$ we observe that when FS is at the upper end of the intermediate scale (FS > 3.7), $\langle g \rangle$ is far from the value of the lower state $\langle g \rangle \approx 0.1$. This indicates that the transition is incomplete and larger values of FS are needed to get the entire system to $\langle g \rangle \approx 0.1$. We conclude that the transition is incomplete when both the added noise and the initial values are large.

3.3. *Values of the spatial auto-correlation function for the bistable regime*

As illustrated by Fig. 4(c), intermediate values of FS lead to an irregular spatial pattern of the conductance values. In this section, we will quantitatively characterize this irregular alternation between low and high conductances. The irregularity will be described in terms of the auto-correlation function. The auto-correlation function $C(\zeta)$ is a tool that characterizes the degree of similarity of a signal with the same signal shifted by a spatial lag usually denoted by ζ [Kantz *et al.*, 1998]. The correlation function C is normalized by the variance such that $C(\zeta = 0) = 1$ and it takes values in the range between -1 and 1 [Kantz *et al.*, 1998]. A value close to 1 indicates a strongly correlated signal and a value close to -1 indicates a strong anti-correlation. Here we must stress that we have used the correlation function in order to get some hints about the typical length scales involved after the system equilibrates towards a quasi-steady state. In case of essentially binary spatial states, autocorrelation function and several information theoretic measures such as mutual information lead to results that are qualitatively identical [Voss *et al.*, 1998]. Here the spatial lag is measured as the number of cells that separates the original and the shifted signal. This implies that $\zeta = 1$ is the lag between two adjacent cells in the cable. For the simulations presented in Fig. 9 the spatial auto-correlation function is computed at the final stage of the simulations. Figure 10 displays examples of auto-correlation functions for three sets of parameters. The blue line corresponds to parameters $(\text{FS}; g_{\rm ini}; N_s) = (1.55; 0.1; 0)$. Its slow decay indicates that the signal is highly correlated in space. Indeed, the conductance values are almost constant in space.

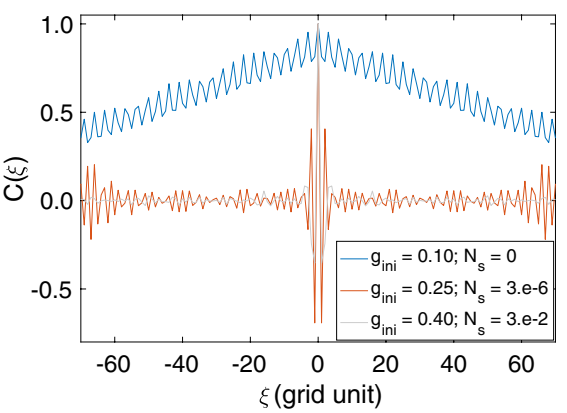

Fig. 10. Three examples of the spatial auto-correlation function of the spatial gap junction signal (i.e. the conductance values of the cable) taken at the end of the simulation (after 2000 beats). The three cases shown correspond to the parameters: $g_{\rm ini} = 0.1; N_s = 0$ (blue line); $g_{\rm ini} = 0.25; N_s = 3 \cdot 10^{-6}$ (red line); $g_{\rm ini} = 0.4; N_s = 3 \cdot 10^{-2}$ (gray line). Note that we have fixed the shrinking factor to FS $= 1.55$ in all three cases.

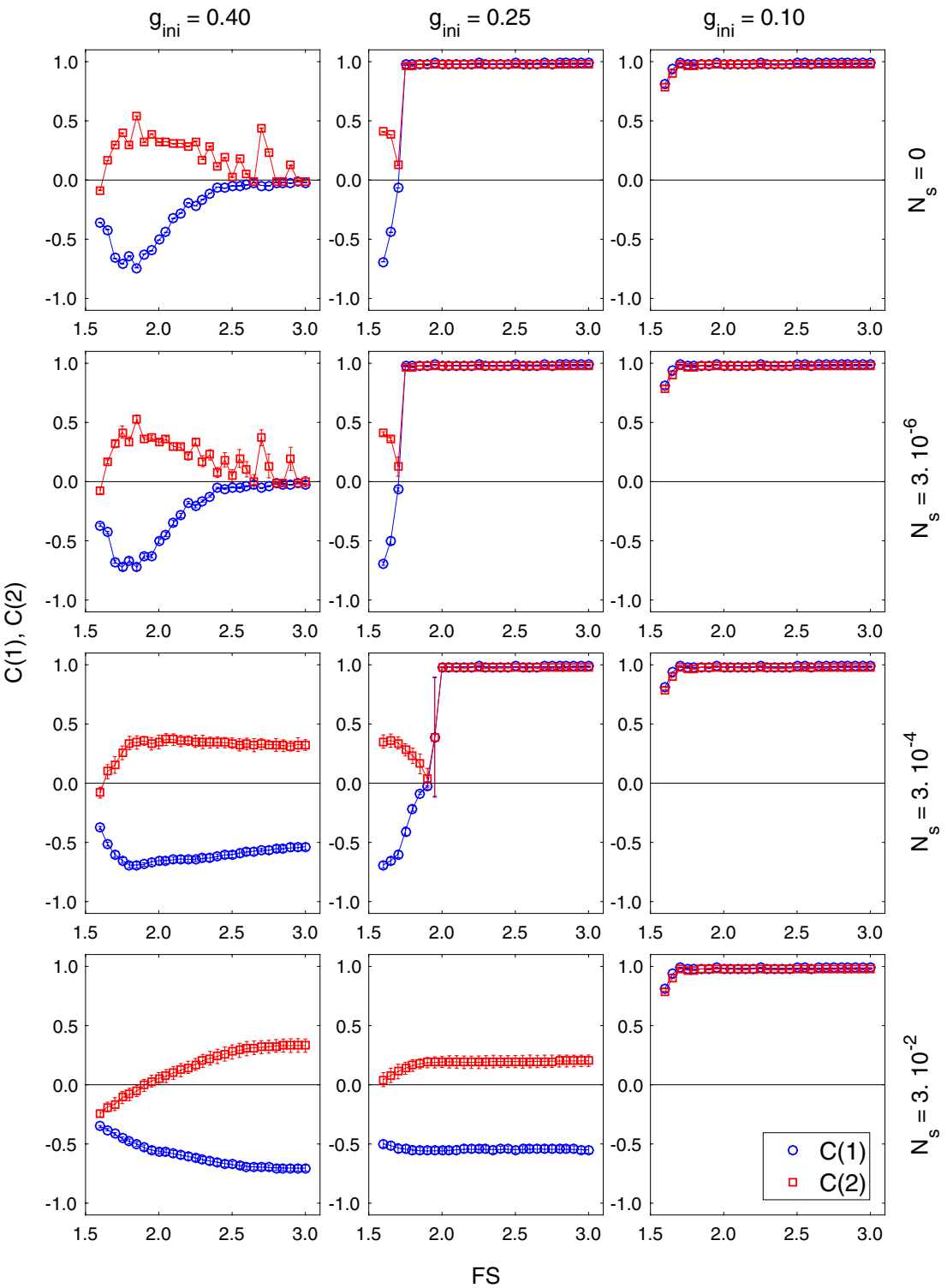

Fig. 11. Composite figure in each panel shows lag one $C(\zeta = 1)$ (blue circles) and lag two $C(\zeta = 2)$ (red squares) values (vertical axis) of the spatial auto-correlation function for the conductance vector g_i as a function of the shrinking factor FS (horizontal axis). Two parameters are associated with each panel. The noise strength is varied with the panel's row: $N_s = \{0; 3\cdot10^{-6}; 3\cdot10^{-4}; 3\cdot10^{-2}\}$ (top to bottom). The initial GJ value $g_{\rm ini}$ is varied with the panel's column: $g_{\rm ini} = \{0.4; 0.25; 0.1\}$ (left to right). Here we show the average values (symbols) plus/minus the standard deviations (error bars) based on 15 independent random realizations of the initial added noise.

In the specific case considered here, the signal (i.e. the conductance values of the cable) has essentially two different values. This allows a probabilistic interpretation of the correlation function. If its value is positive (for a specific lag) this means that there is an enlarged probability (compared to the average probability of that conductance) that the lagged conductance has the same value as the considered one. The higher the value of the correlation function the more likely it is that the two conductances coincide. In case of the maximum possible value ($C(\zeta) = 1$) this probability is equal to 1. However, if the value of the correlation function is negative the lagged conductance is more likely to have the alternative value of conductance. For many parameters of the model we observe that $C(1) < 0$ and $C(2) > 0$. This indicates a highly fluctuating behavior of the conductance (sawtooth pattern). A more negative value of the correlation function at $C(1)$ indicates a more regular alternating pattern.

The examination of few examples of auto-correlation functions (presented in Fig. 10) indicates that for the purpose of the present analysis we can restrict the study of the auto-correlation functions to the values given at lag one $C(\zeta = 1)$ and lag two $C(\zeta = 2)$. Figure 11 reports these values for the same set of model parameters used in Fig. 9. The value of the correlation function at $\zeta = 1$ is presented as blue circles and for $\zeta = 2$ as red squares. In case of (almost) constant conductances, both values approach 1. This corresponds to the blue curve in Fig. 10. For the mixed state, we find both values smaller than 1. In most cases we find $C(1) < 0$ and $C(2) > 0$, which stands for the presence of a sawtooth pattern (see also the red curve in Fig. 10). The higher the absolute difference between $C(1)$ and $C(2)$ the better is the alternans pattern. This oscillating behavior is thus found for large values of G_{ini} and for high initial noise strengths. For a small part of the parameter space both values of the autocorrelation function are negative. Here we expect the conductance to vary upon a larger spatial scale.

4. Conclusions

This paper has presented simulations of a model of cardiac tissue that includes the dynamics of the connexins in the gap junctions separating the cardiac myocytes. Previous studies have shown that in the normal (healthy) regime the conductance value remains almost constant, with very small variations during a stimulation. Here we have set the model parameters in a diseased state by modifying the model in three steps: (a) an overall reduction of the conductance (mimicking an ischemic tissue); (b) a reduction of the upper plateau of the connexin characteristics (quantified here by the shrinking factor FS); (c) a modification of the time scale associated with the connexin dynamics. All these modifications can be somewhat physiologically justified but are rarely present at once in an experiment. Our simulations have revealed an interesting bifurcation between high and low level of conductance mediated by the parameter FS, resulting in dynamic down regulation of gap junction conductance [Willy *et al.*, 2017]. Furthermore, the spatial distribution during the transition is not uniform but exhibits a very highly alternating dynamics. We have quantified the observed transition through several indicators as the mean conductance (order parameter) and the spatial auto-correlation function (similar to a structure function).

The presented study is based on some simplifications. The corresponding limitations will be addressed in future works. The cardiac tissue is certainly not one-dimensional and one has to adapt the model to a system with higher spatial dimension. The coupling between the cardiomyocytes by gap junctions should be modeled in a more complex way such that on average each cardiomyocyte is coupled to 11 others. Of particular interest would be the study of the spiral wave stability in a system with included connexin dynamics. Furthermore, the described bifurcation should be analytically tracked down, by using tools from bifurcation analysis.

Acknowledgments

The authors acknowledge financial support from the Spanish Ministerio de Economía y Competitividad (MINECO) under Grant Nos. SAF2014-58286-C2-2-R and SAF2017-88019-C3-2-R and from the Fundació La Marató de TV3. D. Laroze acknowledges the partial financial support from Centers of Excellence with BASAL/CONICYT financing, Grant No. FB0807, CEDENNA, CONICYT-ANILLO ACT 1410, and FONDECYT 1180905. C. Hawks also thanks "Asociación de Amigos de la Universidad de Navarra" for her fellowship.

References

Aguel, F., Eason, J. & Trayanova, N. [2003] "Advances in modeling cardiac defibrillation," *Int. J. Bifurcation and Chaos* **13**, 3791–3803.

Asimaki, A. & Saffitz, J. E. [2012] "Gap junctions and arrhythmogenic cardiomyopathy," *Heart Rhythm* **9**, 992–995.

Beardslee, M. A., Lerner, D. L., Tadros, P. N., Laing, J. G., Beyer, E. C., Yamada, K. A., Kléber, A. G., Schuessler, R. B. & Saffitz, J. E. [2000] "Dephosphorylation and intracellular redistribution of ventricular connexin43 during electrical uncoupling induced by ischemia," *Circul. Res.* **87**, 656–662.

Bennett, M., Barrio, L., Bargiello, T., Spray, D., Hertzberg, E. & Saez, J. [1991] "Gap junctions: New tools, new answers, new questions," *Neuron* **6**, 305–320.

Beutler, B. [2018] "Mutagenetix (tm)," https://mutagenetix.utsouthwestern.edu.

Boengler, K. & Schulz, R. [2018] "Connexins in cardiac ischemia," *Curr. Opin. Physiol.* **2**, 123–128.

Bragard, J. [2018] "Connexins dynamics animations," http://fisica.unav.es/˜jbragard/research100.html.

Bukauskas, F. F., Bukauskiene, A., Verselis, V. K. & Bennett, M. V. [2002] "Coupling asymmetry of heterotypic connexin 45/connexin 43-egfp gap junctions: Properties of fast and slow gating mechanisms," *Proc. Natl. Acad. Sci. USA* **99**, 7113–7118.

Cantalapiedra, I. R., Peñaranda, A., Echebarria, B. & Bragard, J. [2010] "Phase-2 reentry in cardiac tissue: Role of the slow calcium pulse," *Phys. Rev. E* **82**, 011907.

Cantalapiedra, I. R., Penaranda, A. & Echebarria, B. [2014] "Propagation malfunctions due to gap junction dysregulation," *Computing in Cardiology Conf. (CinC), 2014* (IEEE), pp. 1045–1048.

Cherry, E. M., Fenton, F., Krogh-Madsen, T., Luther, S. & Parlitz, U. [2017] "Introduction to focus issue: Complex cardiac dynamics," *Chaos* **27**, 3701.

Costa, C. M., Silva, P. A. A. & dos Santos, R. W. [2016] "Mind the gap: A semicontinuum model for discrete electrical propagation in cardiac tissue," *IEEE Trans. Biomed. Engin.* **63**, 765–774.

Delmar, M. & Makita, N. [2012] "Cardiac connexins, mutations and arrhythmias," *Curr. Opin. Cardiol.* **27**, 236–241.

Desplantez, T., Halliday, D., Dupont, E. & Weingart, R. [2004] "Cardiac connexins cx43 and cx45: Formation of diverse gap junction channels with diverse electrical properties," *Pflugers Arch.* **448**, 363–375.

Desplantez, T., Dupont, E., Severs, N. & Weingart, R. [2007] "Gap junction channels and cardiac impulse propagation," *J. Membr. Biol.* **218**, 13–28.

Donnell, P., Baigent, S. A. & Banaji, M. [2009] "Monotone dynamics of two cells dynamically coupled by a voltage-dependent gap junction," *J. Theoret. Biol.* **261**, 120–125.

Dunn, C. A. & Lampe, P. D. [2014] "Injury-triggered akt phosphorylation of cx43: A zo-1-driven molecular switch that regulates gap junction size," *J. Cell Sci.* **127**, 455–464.

Fenton, F. & Karma, A. [1998] "Vortex dynamics in three-dimensional continuous myocardium with fiber rotation: Filament instability and fibrillation," *Chaos* **8**, 20–47.

Glukhov, A. V., Fedorov, V. V., Kalish, P. W., Ravikumar, V. K., Lou, Q., Janks, D., Schuessler, R. B., Moazami, N. & Efimov, I. R. [2012] "Conduction remodeling in human end-stage non-ischemic left ventricular cardiomyopathy," *Circulation* **125**, 1835–1847.

Gokhale, T. A., Medvescek, E. & Henriquez, C. S. [2017] "Modeling dynamics in diseased cardiac tissue: Impact of model choice," *Chaos* **27**, 093909.

Grandi, E., Pasqualini, F. S. & Bers, D. M. [2010] "A novel computational model of the human ventricular action potential and CA transient," *J. Molecul. Cell. Cardiol.* **48**, 112–121.

Gutstein, D. E., Morley, G. E., Vaidya, D., Liu, F., Chen, F. L., Stuhlmann, H. & Fishman, G. I. [2001] "Heterogeneous expression of gap junction channels in the heart leads to conduction defects and ventricular dysfunction," *Circulation* **104**, 1194–1199.

Hand, P. E. & Griffith, B. E. [2010] "Adaptive multiscale model for simulating cardiac conduction," *Proc. Natl. Acad. Sci. USA* **107**, 14603–14608.

Hawks, C., Elorza Barbajero, J., Echebarria Dominguez, B., Rodriguez Cantalapiedra, I., Penaranda Ayllon, A. & Bragard, J. [2015] "Influence of gap junction dynamics on the stability of reentrant waves in cadiac tissue," *Comput. Cardiol.* **42**, 437–440.

Hsieh, Y.-C., Lin, J.-C., Hung, C.-Y., Li, C.-H., Lin, S.-F., Yeh, H.-I., Huang, J.-L., Lo, C.-P., Haugan, K., Larsen, B. D. *et al.* [2016] "Gap junction modifier rotigaptide decreases the susceptibility to ventricular arrhythmia by enhancing conduction velocity and suppressing discordant alternans during therapeutic hypothermia in isolated rabbit hearts," *Heart Rhythm* **13**, 251–261.

Imanaga, I. [2010] "Pathological remodeling of cardiac gap junction connexin43 with special reference to arrhythmogenesis," *Pathophysiology* **17**, 73–81.

Jalife, J., Morley, G. E. & Vaidya, D. [1999] "Connexins and impulse propagation in the mouse heart," *J. Cardiovascul. Electrophysiol.* **10**, 1649–1663.

Kantz, H., Kurtz, J. & Mayer-Kress, G. E. [1998] *Nonlinear Analysis of Physiological Data* (Springer, Berlin).

Keener, J. P. [1991] "The effects of discrete gap junction coupling on propagation in myocardium," *J. Theoret. Biol.* **148**, 49–82.

Keener, J. & Sneyd, J. [1998] *Mathematical Physiology* (Springer-Verlag, NY).

Kostin, S., Rieger, M., Dammer, S., Hein, S., Richter, M., Klövekorn, W.-P., Bauer, E. P. & Schaper, J. [2003] "Gap junction remodeling and altered connexin43 expression in the failing human heart," *Cardiac Cell Biology* (Springer), pp. 135–144.

Lin, X., Crye, M. & Veenstra, R. D. [2003] "Regulation of connexin43 gap junctional conductance by ventricular action potentials," *Circul. Res.* **93**, e63–e73.

Noureldin, M., Chen, H. & Bai, D. [2018] "Functional characterization of novel atrial fibrillation-linked gja5 (cx40) mutants," *Int. J. Molecul. Sci.* **19**, 977.

Peters, N. S. & Wit, A. L. [1998] "Myocardial architecture and ventricular arrhythmogenesis," *Circulation* **97**, 1746–1754.

Qu, Z. [2014] "Network dynamics in cardiac electrophysiology," *Systems Biology of Metabolic and Signaling Networks* (Springer), pp. 243–260.

Sachse, F. B. [2004] *Computational Cardiology: Modeling of Anatomy, Electrophysiology, and Mechanics* (Springer, Berlin).

Sachse, F. B., Moreno, A. P. & Abildskov, J. [2008] "Electrophysiological modeling of fibroblasts and their interaction with myocytes," *Ann. Biomed. Engin.* **36**, 41–56.

Santos-Miranda, A., Noureldin, M. & Bai, D. [2018] "Effects of temperature on transjunctional voltage-dependent gating kinetics in cx45 and cx40 gap junction channels," *J. Molecul. Cell. Cardiol.* **127**, 185–193.

Schulz, R., Görge, P. M., Görbe, A., Ferdinandy, P., Lampe, P. D. & Leybaert, L. [2015] "Connexin43 is an emerging therapeutic target in ischemia/reperfusion injury, cardioprotection and neuroprotection," *Pharmacol. Therap.* **153**, 90–106.

Severs, N. J., Bruce, A. F., Dupont, E. & Rothery, S. [2008] "Remodelling of gap junctions and connexin expression in diseased myocardium," *Cardiovascul. Res.* **80**, 9–19.

Shaw, R. M. & Rudy, Y. [1997] "Ionic mechanisms of propagation in cardiac tissue: Roles of the sodium and l-type calcium currents during reduced excitability and decreased gap junction coupling," *Circul. Res.* **81**, 727–741.

Spach, M. S., Heidlage, J. F., Dolber, P. C. & Barr, R. C. [2000] "Electrophysiological effects of remodeling cardiac gap junctions and cell size: Experimental and model studies of normal cardiac growth," *Circul. Res.* **86**, 302–311.

Ten Tusscher, K., Noble, D., Noble, P.-J. & Panfilov, A. V. [2004] "A model for human ventricular tissue," *Amer. J. Physiol.-Heart and Circul. Physiol.* **286**, H1573–H1589.

Tse, G. & Yeo, J. M. [2015] "Conduction abnormalities and ventricular arrhythmogenesis: The roles of sodium channels and gap junctions," *IJC Heart Vascul.* **9**, 75–82.

Van Norstrand, D. W., Asimaki, A., Rubinos, C., Dolmatova, E., Srinivas, M., Tester, D. J., Saffitz, J. E., Duffy, H. S. & Ackerman, M. J. [2012] "Connexin43 mutation causes heterogeneous gap junction loss and sudden infant death," *Circulation* **125**, 474–481.

Verheule, S. & Kaese, S. [2013] "Connexin diversity in the heart: Insights from transgenic mouse models," *Front. Pharmacol.* **4**, 81.

Vogel, R. & Weingart, R. [1998] "Mathematical model of vertebrate gap junctions derived from electrical measurements on homotypic and heterotypic channels," *J. Physiol.* **510**, 177189.

Voss, H., Bunner, M. J. & Abel, M. [1998] "Identification of continuous, spatiotemporal systems," *Phys. Rev. E* **57**, 2820–2823.

Willy, G. Y., Yue, B., Aoyama, H., Kim, N. K., Cameron, J. A., Chen, H. & Bai, D. [2017] "Junctional delay, frequency, and direction-dependent uncoupling of human heterotypic cx45/cx43 gap junction channels," *J. Molecul. Cell. Cardiol.* **111**, 17–26.